Engineering Fracture Mechanics 114 (2013) 92–103

Contents lists available at ScienceDirect

Engineering Fracture Mechanics

journal homepage: www.elsevier.com/locate/engfracmech

Comprehensive concrete fracture tests: Description and results

Christian G. Hoover [a,1], Zdeněk P. Bažant [b,*], Jan Vorel [a,2], Roman Wendner [a], Mija H. Hubler [a]

[a] Northwestern University, 2145 Sheridan Road, Evanston, IL 60208, USA
[b] Civil Engineering and Materials Science, Northwestern University, 2145 Sheridan Road, CEE/A135, Evanston, IL 60208, USA

ARTICLE INFO

Article history:
Received 7 February 2013
Received in revised form 25 July 2013
Accepted 3 August 2013

Keywords:
Concrete fracture
Scaling of strength
Fracture testing
Statistical scatter
Notch depth effect
Flexural strength
Modulus of rupture

ABSTRACT

Although hundreds of concrete fracture tests exist, their evaluation is ambiguous because they have limited ranges of specimen size, initial notch depth and postpeak response, and refer to different concretes, different batches of concrete, different ages, different environmental conditions, different loading rates and test procedures, and different specimen types. Presented is an experimental investigation of unprecedented comprehensiveness and low scatter, using specimens made from one batch of concrete. It includes: (1) notched and unnotched beams tested at virtually the same age; (2) crack depths ranging from 0% to 30% of beam depth; (3) a broad size range (1: 12.5); (4) tests in transition between type 1 and type 2 size effects; (5) virtually complete postpeak softening data; (6) properly correlated loading rates; and (7) complete standard characterization of the concrete used. The analysis is relegated to a follow-up paper.

1. Introduction

Although the literature abounds with reports on many hundreds of concrete fracture tests [e.g., 1–11,34], a consensus on the modeling of fracture and its consequences is still elusive and different competing models happily survive alongside, impeding the introduction of fracture concepts into concrete design and codes.

One reason for the lack of consensus is that all of these fracture tests have explored only rather limited ranges of the relevant influencing parameters such as the specimen size, initial notch depth and postpeak response, and have been performed on different concretes, on different batches of supposedly the same concrete, at different ages, at different environmental conditions, at different rates, with different test procedures, and on specimens of different types and dimensions. Aggregated evaluations of the available data have been attempted, yet with little success since the fracture characteristics have been drowned in great uncertainties and scatter due to the effects of the aforementioned influencing parameters and test conditions, without which a clear interpretation of the available data is impossible.

To overcome these problems, the US Department of Transportation provided major funding to conduct a series of concrete fracture tests of unprecedented scope. All the specimens were made from the same batch of concrete, were of virtually the same age, and all went through the same curing regimen and the same environmental conditions during the test. All samples were tested in the same manner with a stable mode of control using the same closed-loop servo-controlled machines, and at rates ensuring about the same time to reach the peak load. Altogether, 128 fracture specimens were cast

* Corresponding author. Tel.: +1 847 491 4025; fax: +1 847 491 4011.
E-mail addresses: christianhoover2010@u.northwestern.edu, orcgh2@mit.edu (C.G. Hoover), z-bazant@northwestern.edu (Z. P. Bažant), jan.vorel@fsv.cvut.cz (J. Vorel), r-wendner@northwestern.edu (R. Wendner), m-hubler@u.northwestern.edu (M.H. Hubler).
[1] Present affiliation: Massachusetts Institute of Technology, Cambridge, MA 02139, USA.
[2] On leave from Faculty of Civil Engineering, Czech Technical University in Prague, Thakurova 7, 16629 Prague CTU in Prague.

0013-7944/$ - see front matter © 2013 Elsevier Ltd. All rights reserved.
http://dx.doi.org/10.1016/j.engfracmech.2013.08.007

simultaneously in precision-crafted molds, and further 36 companion specimens were cast simultaneously from the same batch to determine the basic characteristics of the concrete used, such as the compressive strength, modulus of rupture, Young's modulus and Poisson's ratio.

The present tests resulted in a very large amount data, the analysis of which will require several papers, and which will also serve other investigators to check their models. What can be done in this first paper (summarized at a recent conference; [12]), is to present the main test results and check the trends of data, while numerous additional details which might be needed by other researchers for reproducing the tests or for reanalyzing the data are posted on a website; see [http://www.civil.northwestern.edu/people/bazant/].

An especially important gap of knowledge, which has, for example, hampered a critical appraisal of the Hu-Duan boundary effect model [13–18], exists in the transition between the Type 1 and Type 2 size effects. The Type 1 size effect occurs in structures that have no notches nor preexisting large cracks and fail right after the initiation of a macro-crack from a smooth surface. The Type 2 size effect occurs when either a deep notch or a long stress-free crack has grown in a stable manner before reaching the maximum load (as is typical of reinforced concrete). In Type 2, the size effect curve terminates with the power law $D^{-1/2}$ (where D = structure size, here taken as the beam depth), while in Type 1 it terminates either with a horizontal asymptote if the statistical size effect is negligible or, otherwise with a power law characterized by a negative exponent of a much smaller value than $-1/2$, which represents the steepest slope possible according to LEFM. In Type 2 asymptotic behavior, the notch or pre-existing macro-crack is much larger than the fracture process zone (FPZ), while in Type 1 the macro-crack at maximum load is approximately of the size of the FPZ. The FPZ of quasibrittle materials undergoes softening behavior due to distributed damage such as micro-cracking and softening frictional slip, which may be described by a softening stress-separation relation of a cohesive crack model. A key objective of this study is to determine the transition between types 1 and 2. To this end, shallow initial notches with a depth comparable to the FPZ size have been included in the test program.

The importance of comprehensiveness of fracture test data has been highlighted by several recent studies. For instance, when the work-of-fracture test (for concrete also known as Hillerborg's test [19], standardized by RILEM [20]) is conducted on specimens of only one size, the determination of the bilinear cohesive softening law is, as recently shown [21], highly non-unique. The test results can be fitted equally well with bilinear softening laws whose tensile strength limit differs by as much as 70% and the initial fracture energy by 68%. Similar ambiguities have been demonstrated in a recent critique of the Hu-Duan boundary effect model [22,35].

When, however, the complete softening curves are known for several very different sizes, the identification of the bilinear softening laws becomes closer to being unique. Likewise, when only the size effect on the nominal strength is tested, the complete bilinear softening law of concrete cannot be identified uniquely, but if the postpeak response measurements are included, the non-uniqueness gets mitigated or wiped out. Furthermore, when the tests at different notch depths do not include the case of zero notch depth and very different sizes, the same data can be fitted by very different models, e.g., the size effect law, the Hu-Duan model [13–18] or Carpinteri's 'multifractal scaling law' [7,23]. But the data fit becomes unique when the zero notch depth is included [36,37]. Many other ad hoc size effect models, unrelated to fracture tests, have been introduced for special structural applications, such as the CEB model [24], the JSCE model [25] and Collins's model [26–29] for the size effect in shear failure of reinforced concrete beams, or the Swiss code model for size effect in punching shear (cf. [30]).

Concrete is an archetypical example of quasibrittle (or brittle heterogeneous) materials, which also include fiber composites, tough ceramics, various rocks, stiff soils, sea ice, rigid foams, dental ceramics, wood, carbon, bone, many biological materials and brittle materials on the micrometer scale. Unlike brittle materials, the FPZ is not negligible compared to the cross-section dimension and has an effective width equal to about 2 to 3 time the largest inhomogeneity (or aggregate) size. In the large size limit, which is usually way beyond the practical testing range, they behave as perfectly brittle. Because quasibrittle materials consist of brittle constituents, their FPZ exhibits gradual softening damage, which can be described by a softening stress-displacement law of the cohesive crack model and crack band model. This contrasts with ductile fracture of metals, in which the non-linear zone around the crack tip is also large but is plastic rather than softening, while the softening damage is concentrated in a very small FPZ.

The present work fills a glaring gap in the experimental basis of concrete fracture modeling—the lack of comprehensive experimental data, and especially the lack of information on the transition between the Type 1 and 2 size effects. This experimental analysis is reported in [31].

2. Test specimen details

A total of 164 concrete specimens were cast within three hours on January 27th, 2011. They were all cast from the same batch of continually mixed concrete, which ensured the material properties of all the specimens to be virtually the same. The casting included 128 beams of 4 different sizes (Table 1), all geometrically similar, and also 24 cylinders of diameter 3 in. (76.2 mm) and length 6 in. (152.4 mm) and 12 ASTM standard flexural test beams of width and height 6 in. (152.4 mm), and length 22 in. (558.8 mm). The thickness of all other 128 beams was 1.58 in. (40 mm) and the length-to-depth ratio was 2.4. The beam depths were 1.58, 3.66, 8.47 and 19.69 in. (40, 93, 215 and 500 mm), corresponding to a size range of 1: 12.5; see Fig. 1 and Table 1.

Table 1
Geometry and quantities of beams of each family.

Relative size	Depth × length, mm	Relative notch depth, α_0					Total quantities
		0	0.025	0.075	0.15	0.3	
12.5	500 × 1200	6	6	6	6	6	30
5.386	215 × 516	6	6	6	6	6	30
2.321	93 × 223.2	8	0	8	8	8	32
1	40 × 96	7	0	11	10	8	36

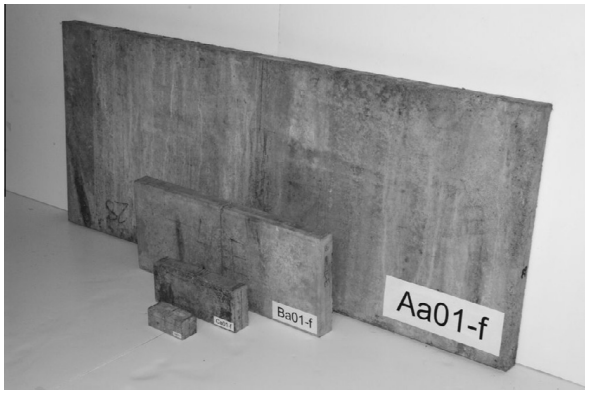

Fig. 1. Isometric view of different sizes of beams, $\alpha_0 = 0.3$.

Notches of 0.06 in. (1.5 mm) wide and five different relative depths $\alpha = a/D = 0$, 0.025, 0.075, 0.150 and 0.300, were cut into the beams (where a = notch depth) with a diamond band saw. The beam labeling was as follows: the capital letter designates the beam size, 'A' the largest through 'D' the smallest; the subsequent lower case letter designates the relative notch depth, 'a' standing for $\alpha = 0.3$ through 'e' for $\alpha = 0$; the following is the beam number, and either '-f' for the beam face against the mold or '-b' for the screeded face. Beam families of 18 different geometries (denoted by the combination of the first two letters of the beam label) were cast, with no less than 6 specimens per geometry; see Table 1.

To detect any variability in the strength of concrete over the casting period, one group of 8 cylinders and 4 ASTM beams was cast at the beginning of casting, a second group about 1.5 h later and the third group at the end of casting. On January 29th, 2011, the specimens were demolded, covered in wet burlap and placed in a curing room of 100% humidity and temperature about 25 °C. Every day the beams were checked to ensure they were kept moist. The specimens were kept in the curing room for about 13 months, which ensured negligible influence of aging effects during the testing period. All the notches were cut in the beams during the week of May 2, 2011, 96 days after casting. The beams were kept moist the whole time except briefly when the notches were drawn and cut.

3. Description of tests

3.1. Material

A ready-mixed concrete (delivered from Ozinga Brothers, Inc), was used. The specified compressive strength was 4500 psi (31.03 MPa). The coarse aggregate was pea gravel, consisting of glacial outwash deposits from McHenry, Illinois, with the maximum aggregate diameter of 0.39 in. (10 mm). The water-cement ratio was 0.41 and the water-binder ratio was 0.35. A slump retention admixture was added, not only to delay hydration but also to guarantee workability for the full 3 h duration of casting. No slump tests were performed, but the digital slump meter on the concrete truck measured a consistent 6 in. slump throughout the duration of the casting period.

Precision molds for the beams were built using Douglas fir and medium density overlay (MDO) plywood, except for the sides of the molds for the smallest beams which were metallic. The cylinder molds were plastic. Prior to placing the concrete, all the wooden surfaces which would contact the concrete were coated with form oil to prevent water from seeping into the pores of the wood and to prevent the concrete from bonding to the wood. The molds were also water-sealed at the joints, so that no water could escape.

3.2. Casting procedure

The beams were cast horizontally with the beam thickness given by the depth of the mold. Vertical casting in narrow and tall molds was initially tried, with the beam depth given by the depth of the mold, but was rejected because of excessive

scatter of test results, due to formation of large air voids and to segregation of the aggregate during vibration towards the bottom of the molds. The horizontal casting ensured that any trapped air would get easily expelled during vibration and that no aggregate segregation would occur along the beam depth. After placing the concrete, the molds were vibrated and any excess fresh concrete was removed by screeding. The exposed surface was smoothed with masonry trowels, and then the beams were covered with plastic and remained untouched for 36 h. All the beams were cast within 3 h.

3.3. Testing machines used

Three MTS closed-loop testing machines, with the capacities of 1,000,000 lb (4.5 MN), 220,000 lb (980 kN) and 20,000 lb (89 kN), were used to test the concrete specimens. In all cases, the stroke (displacement of the piston measured inside the machine), time and force were recorded. At the start of every day, the machines were cycled under stroke control for a few minutes and the load cells were shunt-calibrated to make sure they were responding properly. All the gauges used were also re-calibrated before the testing period began.

3.4. Compliance of testing machines and fixtures

If a sensor measuring deformation is placed between two points on a deforming specimen, then the recorded values are truly the response. However, if one a sensor is placed between the specimen and a reference surface, such as the frame test bed, all information recorded from such sensors cannot be directly used for analysis unless: (1) the displacements of any other deforming entity (i.e. supports, load fixtures, the piston assembly) are subtracted from the overall response, or (2) these entities are included in the analysis. As an example, the stroke cannot be equated to the displacement of a specimen because it also contains displacements of the loading fixtures, the piston and any deformations in the machine itself. For this reason, the compliance of all testing machines and loading fixtures used was measured and summarized in Table 2. Two sets of supports were used for each testing machine, one for each beam size.

4. Testing of standard material characteristics

4.1. Initial strength of control cylinders and prisms

12 cylinders, 4 from each casting group, were tested 31 days after casting under stroke control to obtain the standard compressive strength f'_c. A 110,000 lb (490 kN) capacity load cell was used to provide a higher resolution in the force output. The cylinder height, diameter and location of the gauges to be attached were measured and recorded. The cylinders were then capped with a sulfur compound, to ensure that the end cross-sections be parallel, smooth, free of defects and orthogonal to the central loading axis of the testing machine. The capped cylinder was placed inside the machine and tested in circumferential expansion (opening) control by a chain guage. The vertical shortening of the cylinder was measured with an extensometer with a 4 in. (101.6 mm) gauge length. The load vs. circumferential opening displacement response of these cylinders is shown in Fig. 3. One of the cylinders reached peak load in about 7.5 min, and all the remaining cylinders in about 3 min.

On the same day, a total of 6 ASTM beams, 2 from each casting group, were also tested under stroke control in the 220,000 lb (980 kN) capacity machine to determine the modulus of rupture, f_r (or flexural strength), as defined in ASTM standard C293/C293-10 [32]. In accordance with this standard, the orientation of the beams in the machine was such that the screeded surface would not be in contact with any of the loading points; see Fig. 2. The load vs. stroke responses of the ASTM beams are shown in Fig. 3. After the test, the width and height of the failure surface perpendicular to the beam axis were recorded and used to calculate $f_r = 3PS/2bD^2$. The values of compressive strength and modulus of rupture are summarized in Table 3. The 28-day compressive strength can be calculated from the ACI adjustment formula [33]: $f'c_{28} = 6607.5$ psi (45.56 MPa).

All the other cylinders and ASTM specimens remained in the curing room until the time of testing the size effect beams. One of the cylinders failed at a significantly lower strength than the others and, based on the Grubbs outlier detection test, was subsequently not included in the results shown in Table 3. Table 4 presents the mean values of f'_c and f_r and how they

Table 2
Compliance of testing machines and fixtures.

Machine capacity	Beam depth	Compliance (mm/kN)	
		Machine	Fixtures
20 kip (89 kN)	40 mm	0.0219	0.0196
20 kip (89 kN)	93 mm	0.0174	0.00805
220 kip (980 kN)	215 mm	0.00913	0.00448
220 kip (980 kN)	500 mm	0.0068	0.00301

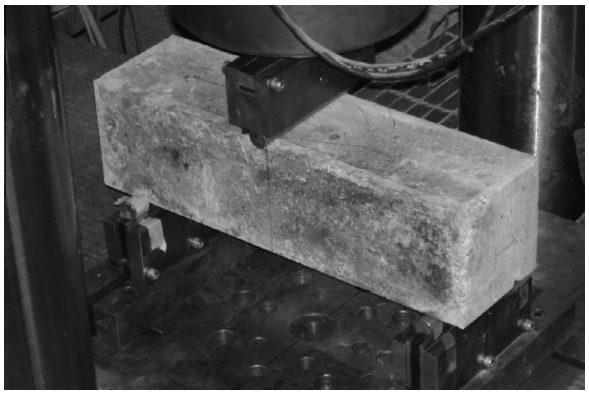

Fig. 2. ASTM beam loaded in 220,000 lb (980 kN) capacity machine.

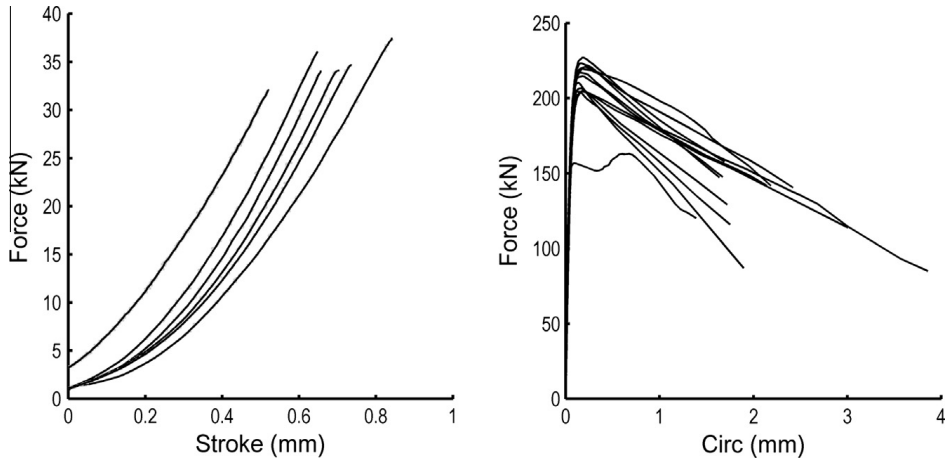

Fig. 3. Results of control tests at age 31 days. Left: load vs. stroke for ASTM beams. Right: load vs. circumferential opening expansion of cylinders.

Table 3
Properties calculated from cylinders and ASTM beams (f_r = modulus of rupture or flexural strength).

	31 day strength		400 day strength			
	f'_c psi (MPa)	f_r psi (MPa)	f'_c psi (MPa)	f_r psi (MPa)	E Msi (GPa)	v
Mean	6749 (46.53)	973.4 (6.72)	8064 (55.6)	1203 (8.29)	5.98 (41.24)	0.172
St.dev.	216.1 (1.49)	50.8 (0.35)	300.6 (2.07)	40.5 (0.28)	0.29 (2.01)	0.017
CoV (%)	3.2	5.22	3.73	3.36	4.87	10.01

varied due to differences in casting times (the specimens marked group 'A', 'B' and 'C' were cast at the beginning, middle and end of the casting period, and the values shown, only differing by a few percent, are the means of all specimens tested from those groups). The small differences, of only a few percent, indicate negligible influence of casting times and a highly uniform concrete mix.

Table 4
Properties calculated from cylinders and ASTM beams poured at (A) beginning, (B) middle and (C) end of casting, 31 day strength.

	f'_c psi (MPa)	f_r psi (MPa)
A	6797 (46.86)	954.8 (6.58)
B	6826 (47.06)	1003 (6.91)
C	6637 (45.76)	962.8 (6.64)

4.2. Concurrent tests of ASTM prisms and cylinders at terminal age

To determine the increase in strength parameters, the remaining cylinders and ASTM beams were tested within two days beginning 400 days after casting (on March 3, 2012), at the halfway point of the fracture tests. The ASTM beams were tested the same way as before ensuring that all the beams reached the peak load in about 3.5 min. The mode of control for the compression cylinders was switched from stroke to circumferential expansion. One cylinder reached the peak in about 8.5 min while all remaining cylinders reached peak in about 5 min. Two steel rings were also attached 1 in. from the top and bottom respectively of the cylinder. Four LVDTs, spanning a distance of 4 in. (101.6 mm), were then placed between the two rings at a radial spacing of $\frac{\pi}{2}$ from each other; see Fig. 4, and used to measure the average vertical shortening of the cylinder. The vertical metal piece in Fig. 4 was used to ensure that the rings were properly spaced. This piece was removed from the assembly once the rings were in place and before the cylinder was placed inside the machine. The vertical displacement, strength and circumferential expansion were then used to calculate Young's modulus and Poisson's ratio; see Table 3. Fig. 6 shows the response of the cylinders and ASTM beams. As can be seen in Table 3, the modulus of rupture increased by the factor of 1.24 and the compressive strength by the factor of 1.19, though the ACI empirical equation for predicting compressive strength due to aging indicates an increase of 1.14 [33].

5. Size effect tests with different notch depths

The main testing period began on February 27th, 2012, and all tests were completed within the span of 11 days, during which the concrete aging due to hydration was negligible compared to the 13-month age of the specimens (it would not have been so if the age were, say, 3 months).

5.1. Testing configuration and instrumentation

The beams of all sizes and notch depths were tested in the closed-loop MTS frames—those of the two smallest sizes in a 20,000 lb (89 kN) capacity frame with a 5000 lb (22 kN) capacity load cell, and those of the larger sizes in the 220,000 lb (980 kN) capacity frame. Small steel loading blocks, of dimensions scaled with the beam size, were glued by cyanoacrylate (superglue) to the beam at the load and support points to prevent local crushing of the concrete from the cylinders on the machine support fixtures; see Fig. 5. All loading blocks were 40 mm wide and the length by height were 60×40, 25.8×17.2, 11.1×7.4 and 4.8×3.2 mm. The bottom two cylinders were resting between the bottom loading blocks and the supports, allowing translation, while the top cylinder was welded to the top fixture. The top and one of the lower supporting fixtures were allowed to rotate about the center of the fixture, but the other support block was fixed against rotation.

The beams of all sizes and notch depths were instrumented with three gauges. The top loading block for all specimens extended about 30 mm on each side of the specimen so that a linear variable differential transformer (LVDT) could be placed against it to measure the vertical displacement of the block on each side of the beam without disturbing the specimen. The LVDTs were firmly supported by stands with magnetic bases which were attached to the test bed. The acquired load-point

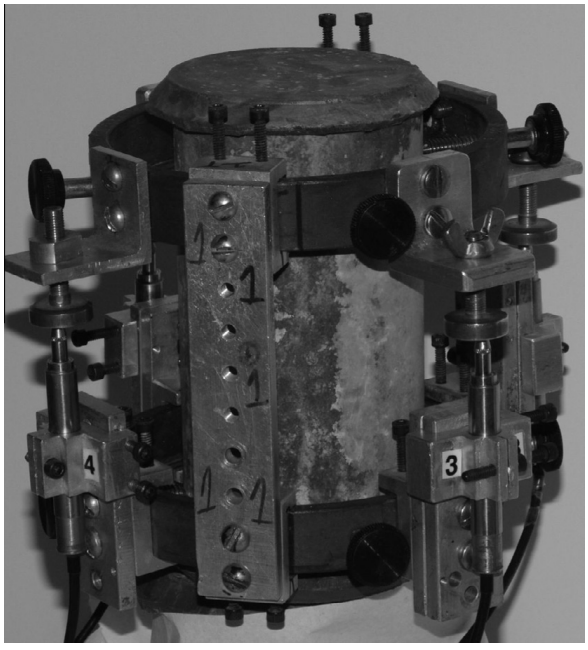

Fig. 4. Sensor array used for testing cylinders, the metal piece was removed before testing.

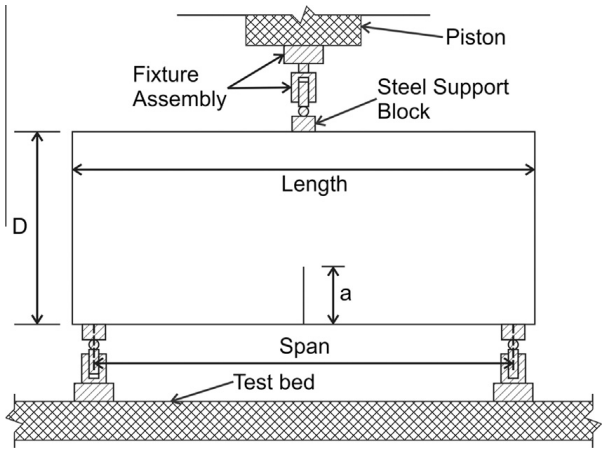

Fig. 5. Loading configuration of beams.

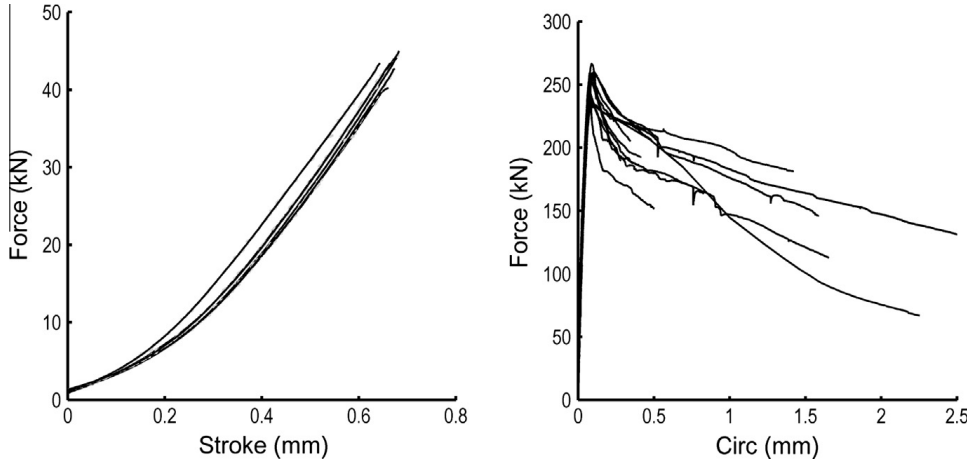

Fig. 6. Results from 400 day testing, on left: load vs. stroke for ASTM beams, on right: load vs. circumferential opening expansion from cylinders.

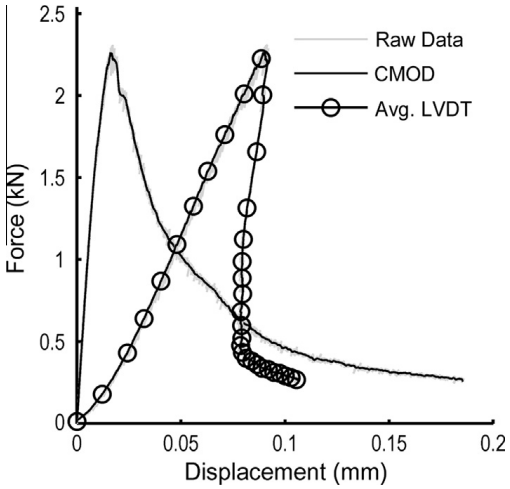

Fig. 7. Load vs. opening displacement and vert. disp. $D = 40$ mm, $\alpha_0 = 0.3$.

displacement data can be used to calculate the work done by the machine on the beam, after subtracting out the contribution of the compliance of the supports, and to make comparisons with finite element models.

All tests were performed under opening displacement control with a prescribed opening velocity of a gauge on the tensile face of the beam. All the beams with $\alpha = 0.3$ were controlled by an extensometer bridging the crack mouth. For beams with

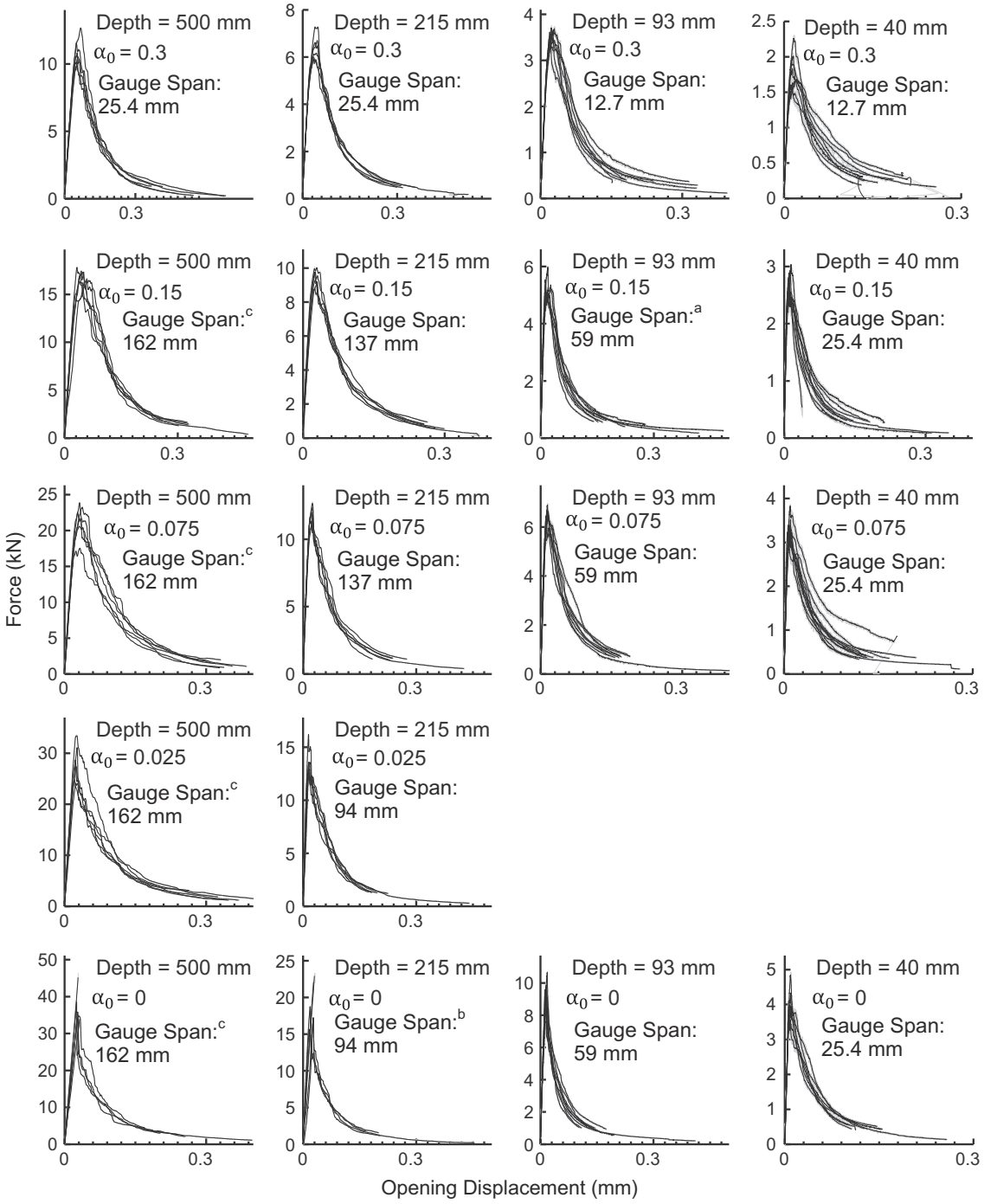

Fig. 8. Force vs. opening displacement graphs for the entire collection of beams. The gauge length was reduced from: (a) 59–25.4 mm, (b) 137.5–94 mm, and (c) 218–162 mm.

no notch or notch shallower than the FPZ, there was some uncertainty as to where the damage would localize into a crack. For control, it was crucial that the crack localized within the gauge length, to avoid snap-down instability. If a crack were to develop outside of the gauge length, the gauge would be closing instead of opening, and the machine would immediately push the piston faster, increasing the closing velocity of the gauge. This cycle would then be rapidly repeated causing the beam to fail suddenly and dynamically, rendering the recorded data useless. Therefore, the tests of all these beams were controlled by either an extensometer with a larger gauge length or by an LVDT spanning a sufficient distance on the tensile face of the beam. It was essential that the gauge continued to open throughout the entire duration of loading to ensure a stable mode of control. When a macrocrack forms, the zone of material near the crack begins to separate as it softens while the rest of the material elastically unloads. If the gauge length is small, and contains the softening zone, the gauge will always open and the test will be stable. However, if the gauge length is too large, the elastically unloading material will cause the gauge to

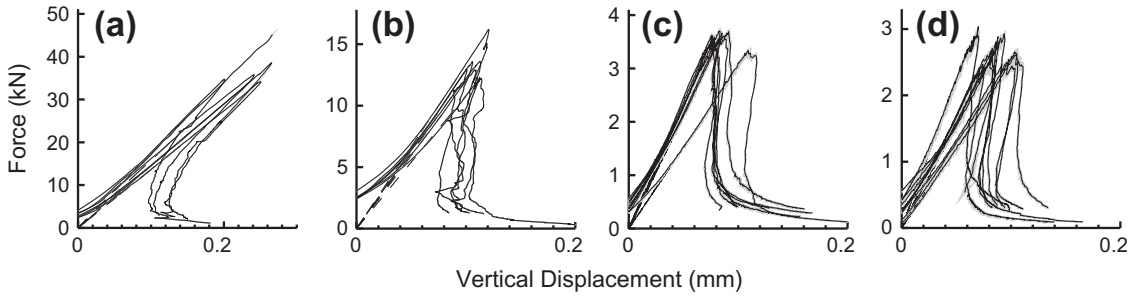

Fig. 9. Collection of force vs. vertical displacement graphs of beam for (a) $D = 500$ mm, $\alpha_0 = 0$, (b) $D = 215$ mm, $\alpha_0 = 0.025$, (c) $D = 93$ mm, $\alpha_0 = 0.3$, (d) $D = 40$ mm, $\alpha_0 = 0.15$.

Table 5
Peak loads and strength of each beam calculated from measured dimensions.

Label	Peak load (kN)	Peak stress (MPa)	Label	Peak load (kN)	Peak stress (MPa)	Label	Peak load (kN)	Peak stress (MPa)	Label	Peak load (kN)	Peak stress (MPa)	Label	Peak load (kN)	Peak stress (MPa)
Aa01	10.80	1.89	Ab01	17.43	2.98	Ac01	23.22	3.95	Ad01	31.13	5.30	Ae01[a]	34.73	4.92
Aa05	10.53	1.85	Ab02	17.34	2.99	Ac02	21.45	3.49	Ad02	24.87	4.31	Aa02[b]	33.94	5.63
Aa06	12.67	2.01	Ab03	15.89	2.84	Ac03	22.50	3.90	Ad03	28.72	5.00	Aa03	34.16	5.83
Aa07	9.90	1.78	Ab04	16.35	2.84	Ac04	23.87	3.96	Ad04	33.41	4.96	Aa04[b]	45.19	5.65
Aa08	10.35	1.80	Ab05	17.82	3.04	Ac05	20.60	3.43	Ad05	24.11	4.02	Ae05	35.79	5.68
Aa09	11.55	1.98	Ab06	16.64	2.86	Ac06	17.54	3.06	Ad06	27.39	4.67	Ae06	38.59	6.36
Ba01	6.17	2.38	Bb01	9.77	3.57	Bc01	11.66	4.64	Bd01	12.98	5.37	Be01	16.65	6.21
Ba02	6.70	2.68	Bb02	9.31	3.69	Bc02	11.02	4.34	Bd02	12.91	5.22	Be02[b]	22.95	8.46
Ba03	6.62	2.61	Bb03	9.74	3.72	Bc03	12.00	4.55	Bd03	13.60	5.41	Be03	17.24	6.23
Ba04	7.28	2.85	Bb04	10.01	3.91	Bc04	12.66	4.99	Bd04	16.21	5.69	Be04[b]	22.09	8.28
Ba05	6.00	2.39	Bb05	8.80	3.48	Bc05	11.59	4.51	Bd05	13.57	5.39	Be05	18.73	6.75
Ba06	5.93	2.40	Bb06	9.21	3.69	Bc06	12.35	4.52	Bd06	12.29	4.86	Be06	15.63	5.99
Ca01	3.33	2.81	Ca08	3.66	3.10	Cb07	5.08	4.31	Cc05	5.97	5.10	Ce03	9.54	7.37
Ca02	3.70	3.13	Cb01	5.97	5.14	Cb08	5.00	4.29	Cc06	6.58	5.58	Ce04	10.67	6.95
Ca03	3.49	2.97	Cb02	5.36	4.73	Cc01	6.47	5.58	Cc07	5.97	5.11	Ce05	9.58	7.40
Ca04	3.62	3.15	Cb03	5.38	4.60	Cc02	6.64	5.52	Cc08	6.89	5.75	Ce06	8.55	7.02
Ca05	3.61	3.03	Cb04	5.53	4.67	Cc03	6.56	5.59	Ce01	9.86	7.78	Ce07	9.41	7.69
Ca06	3.55	3.03	Cb05	5.14	4.38	Cc04	6.66	5.71	Ce02	9.48	7.86	Ce08	9.09	6.74
Ca07	3.69	3.10	Cb06	4.98	4.20									
Da01	1.83	3.71	Db01	2.51	4.94	Db08	2.66	5.29	Dc05	3.34	6.65	De01	3.96	7.62
Da02	1.59	3.11	Db02	2.88	5.75	Db09	2.56	5.08	Dc06	3.52	7.04	De02	4.11	7.56
Da03	1.61	3.22	Db03	2.47	4.93	Db10	3.04	5.99	Dc07	3.83	7.59	De03	3.93	7.32
Da04	1.68	3.39	Db04	2.67	5.43	Dc01	2.99	6.01	Dc08	3.39	6.74	De04	3.92	7.37
Da05	2.26	4.61	Db05	2.63	5.24	Dc02	3.37	6.74	Dc09	3.22	6.36	De05	4.85	8.68
Da06	1.95	3.96	Db06	2.70	5.36	Dc03	3.36	6.68	Dc10	3.33	6.59	De06	4.33	8.57
Da07	2.01	4.10	Db07	2.93	5.82	Dc04	3.17	6.46	Dc12	3.37	6.77	De07	3.62	7.17
Da08	1.68	3.35					30							

[a] The oil pump stopped working during the test, beam was in the machine for a very long time.
[b] Failed dynamically.

close, resulting in snap-down instabilities. The gauge length was initially scaled with the beam size for all specimens, however it was reduced for the two larger size beams to avoid instabilities.

5.2. Test specimen preparation

The beams were kept wet during transportation from the curing room to the testing lab. The actual precise dimensions of each beam were measured on all the six faces of every specimen at multiple locations and the weight of the beam was recorded. The support and instrumentation attachment locations were then marked on the specimen and the steel loading blocks were glued to the beam. The ratio of the span (center-to-center distance of the steel support blocks) to the depth was 2.176. The gauge used for test control was then attached and the beam was placed in the testing machine.

5.3. Testing procedure

The load was set to zero before the piston came in contact with the beam. After a small pre-load, usually between 1–2% of the expected peak load, was placed on the beam, the test began. The motion of the piston was controlled by a constant

Table 6
Coefficients of variation of errors of each family of beams.

α_0	Depth (mm)	Mean, σ_N (MPa)	Std.dev. (MPa)	CoV (%)
0.3	500	1.884	0.095	5.019
0.15	500	2.926	0.088	3.012
0.075	500	3.632	0.366	10.082
0.025	500	4.710	0.476	10.114
0[a]	500	5.6775 (5.956)	0.4629 (0.358)	8.1532 (6.012)
0.3	215	2.551	0.192	7.545
0.15	215	3.678	0.145	3.947
0.075	215	4.591	0.218	4.748
0.025	215	5.323	0.274	5.152
0[a]	215	6.987 (6.295)	1.101 (0.319)	15.758 (5.071)
0.3	93	3.041	0.112	3.695
0.15	93	4.541	0.311	6.846
0.075	93	5.492	0.249	4.541
0	93	7.350	0.414	5.626
0.3[a]	40	3.683 (3.55)	0.514 (0.379)	13.945 (10.68)
0.15	40	5.383	0.367	6.823
0.075	40	6.694	0.397	5.934
0	40	7.756	0.613	7.900

[a] Numbers inside () exclude questionable data points.

opening velocity of the control extensometer bridging the crack mouth. All the beams reached their peak load within about 5–10 min. The test ran until each beam softened below 10% of the peak load, and at least one beam from each family remained in the machine until it had softened below 5%.

6. Size effect tests of beams

6.1. Results

Fig. 7 presents the typical response for a beam 40 mm deep, with $\alpha = 0.3$. The plot shows the evolution of the load as it relates to the crack opening and the average vertical displacement recorded from the LVDTs. The lighter grey area indicates the raw data from the testing machine, and the solid and dashed black lines are the response after the higher frequencies from the testing machine have been filtered out. Fig. 8 shows the entire collection of load versus opening displacement curves for all beams tested, labeled by the corresponding beam depth, the relative crack length α and the span of the gauge used to control the test on the tension face of the beam. Fig. 9 shows a sample of the load versus vertical displacement graphs. All the graphs show very smooth loading paths and good consistency in the pre- and postpeak responses.

The nominal strength $\sigma_N = M(D/2)/I$ where $M = P_u S/4$ = maximum bending moment, $I = b\ D^3/12$ = centroidal moment of inertia (see Table 5) and $\bar{y}$ is the distance from the centroid to the tensile face of the beam. σ_N was calculated for all beams from the measured dimensions, particularly the actual thickness of each beam over the ligament, which deviated slightly from the design thickness of 1.58 in. (40 mm). The average overall thickness for all beams was 1.57 in. (39.74 mm) with the standard deviation of 0.06 in. (1.61 mm) and coefficient of variation (CoV) of 4.06%. The statistics for each family of beams are shown in Table 6. The self-weight bending moment was also added to all the beams. In beams with no notch, the crack location at the bottom face could not be controlled, and so the bending moment M in the cross-section at the true crack location was used in the calculations. Overall, a total of 124 beams exhibited a stable response throughout the entire test duration.

However, beams Aa02, Aa04, Be02 and Be04 failed dynamically. When beam Ae01 was loading, the oil pump overheated and shut off, causing the beam to be stuck under load in the machine for about an hour until the pump turned back on and the test continued. The peak load for beam Da05 is high compared to the rest of the beams in the 'Da' family. Though a Grubb's test showed that it is not a statistical outlier, it was noticed that the cut notch for this beam terminated within a compact group of large aggregates and, after the test, the remaining halves of the beam showed that the crack first had to propagate through the aggregates, which could account for the excessive strength. The statistics for each family containing these beams, given in Table 6, were calculated both with and without inclusion of these questionable values.

6.2. Scatter of results

Considerable care was taken to achieve a low scatter of results, which is important to minimize any ambiguity of theoretical interpretation. This goal has been achieved. The CoV's of errors (defined as the root-mean-square error divided by the mean of data) for all families of beams are listed in Table 6. Compared to previous investigations, in which typically the CoV of errors was between 10% and 15%, these are rather low values. The largest CoV, excluding the questionable data points,

occurs for the 'Da' family, which has a depth of 40 mm and $\alpha = 0.3$. This is expected since, in these beams, the ligament length is only 2.8 times the coarse aggregate diameter.

7. Summary and conclusions

The comprehensiveness and low random scatter of the present experimental investigation of concrete fracture, conducted on specimens which were cast from the same batch of one concrete, should allow a realistic appraisal of various competing models as well as development of better models. The investigated aspects include especially the following:

1. A broad size range, with size ratio 1: 12.5.
2. Complete data on the sensor arrays, loading fixtures and the testing machines, including their compliances.
3. A broad range of notch depths, ranging from zero to 30% of beam depth, and including small notch depths similar to the coarse aggregate size (these data are essential for determining both Type 1 and Type 2 size effects, and the transition between them).
4. Virtually complete postpeak softening diagrams, with strength reduction by at least 90% of peak, and in some cases by more than 95%.
5. Comparable loading rates, reaching the peak loads within 5–10 min.
6. Complete characterization of the concrete used, in terms of standard compression strength tests, flexural strength tests with curves of the load versus the opening displacement, versus the load-point displacement and versus the machine stroke.
7. Virtually the same age of all specimens at the time of test, identical curing and achievement of a low scatter.

Acknowledgements

Financial support from the US Department of Transportation, provided through Grant 20778 from the Infrastructure Technology Institute of Northwestern University, is gratefully appreciated. Special thanks for helping with the planning and conduct of experiments are extended to Jia-Liang Le, Qiang Yu, Kedar Kirane, Mahendra Gattu, Kyung-Tae Kim, Brian Siwek, Abigail Christman, Maya Stuhlbarg, Sam Robinson, Jörg Unger, Shiho Kawashima, Kevin Schwartzenberg, Tracy Yang, Gerald Hoover, Pengkun Hou, Wengui Li, Clayton Hall, Vanja Travaś, Jan Eliáš, Jae Hong Kim, Zoi Metaxa, Sıddık Sener, Mark Beacraft, Steve Albertson, Jeffery Sundwall and Dave Ventre.

References

[1] Becq-Giraudon EF. Size effect on fracture and ductility of concrete and fiber composites. Dissertation, Northwestern Univ.; 2000.
[2] Rocco CG. Size dependence and fracture mechanisms in the diagonal compression splitting test. Ph.D. thesis, Dept. Ciencia de Materiales, Universidad Politecnica de Madrid; 1995.
[3] Sabnis GM, Mirza SM. Size effect in model concretes. J Str Div, ASCE 1979;105:1007–20.
[4] Malvar JL, Warren GE. Fracture energy for three-point-bend tests on single-edge-notched beams. Exp Mech 1988;28(3):266–72.
[5] Nallathambi P. Fracture behaviour of plain concretes. Doctoral dissertation, University of New Castle, Australia; 1986.
[6] Petersson PE. Crack growth and development of fracture zone in plain concrete and similar materials. Report No. TVBM-1006, Div. of Building Materials, Lund Institute of Technology, Lund, Sweden; 1981.
[7] Carpinteri A, Chiaia B, Ferro G. Multifractal scaling law: an extensive application to nominal strength size effect of concrete structures. Atti del Dipartimento di Ingegneria Strutturale, 2 (50). Italy: Politecnico de Torino; 1995.
[8] Bažant ZP, Planas J. Fracture and size effect in concrete and other quasibrittle materials. CRC Press; 1998.
[9] Bažant ZP, Pfeiffer PA. Determination of fracture energy from size effect and brittleness number. ACI Mater J 1987;84(6):463–80.
[10] Tang T, Bažant ZP, Yang S, Zollinger D. Variable-notch one-size test method for fracture energy and process zone length. Engng Fract Mech 1996;55(3):383–404.
[11] Karihaloo BL, Abdalla HM, Xiao QZ. Size effect in concrete beams. Engng Fract Mech 2003;70:979–93.
[12] Hoover CG, Bažant ZP, Wendner R, Vorel J, Hubler M, Kim K, et al. Experimental investigation of transitional size effect and crack length effect in concrete fracture. Life-Cycle and sustainability of civil infrastructure systems: Proceedings of the 3rd International Symposium on Life-Cycle Civil Engineering (IALCCE), Hofburg Palace, Vienna Austria, October 3–6; 2012. in press.
[13] Duan K, Hu X, Wittmann F. Scaling of quasi-brittle fracture: boundary and size effect. Mech Mater 2006;38:128–41.
[14] Hu X. An asymptotic approach to size effect on fracture toughness and fracture energy of composites. Engng Fract Mech 2002;69:555–64.
[15] Hu X, Duan K. Size effect: influence of proximity of fracture process zone to specimen boundary. Engng Fract Mech 2007;74:1093–100.
[16] Hu X, Duan K. Size effect and quasi-brittle fracture: the role of FPZ. Int J Fract 2008;154:3–14.
[17] Hu X, Duan K. Mechanism behind the size effect phenomenon. J Engng Mech 2010;136(1):60–8.
[18] Hu X, Wittmann F. Size effect on toughness induced by crack close to free surface. Engng Fract Mech 2000;65:209–21.
[19] Hillerborg A. The theoretical basis of a method to determine the fracture energy G_F of concrete. Mater Struct 1985;18:291–6.
[20] RILEM. Determination of the fracture energy of mortar and concrete by means of three-point bend tests on notched beams. Mater Struct 1985;18:285–90.
[21] Bažant ZP, Yu Q. Size effect testing of cohesive fracture parameters and non-uniqueness of work-of-fracture method. ASCE J Engng Mech 2011;137(8):580–8.
[22] Yu Q, Le JL, Hoover CG, Bažant ZP. Problems with Hu-Duan boundary effect model and its comparison to size-shape effect law for quasibrittle fracture. J Engng Mech 2010;136(1):40–50.
[23] Carpinteri A, Chiaia B, Ferro G. Size effect on nominal tensile strength of concrete structures: multifractality of material ligament and dimensional transition from order to disorder. Mater Struct 1995;28:311–7.
[24] Comite Euro-International du Beton (CEB). CEB-FIP Model Code 1990; 1991.
[25] Japan Society of Civil Engineers (JSCE). Standard specification for design and construction of concrete structures part I (design), Tokyo; 1991.

[26] Collins MP, Mitchell S, Adebar P, Vecchio FJ. General shear design method. ACI Struct J 1996;93(1):36–45.
[27] Collins MP, Kuchma D. How safe are our large, lightly reinforced concrete beams, slabs and footings? ACI Struct J 1999;96(4):482–90.
[28] Vecchio FJ, Collins MP. The modified compression field theory for reinforced concrete elements subjected to shear. ACI J 1986;83(2):219–31.
[29] Angelakos D, Bentz EC, Collins MP. Effect of concrete strength and minimum stirrups on shear strength of large members. ACI Struct J 2001;98(3):290–300.
[30] Bažant ZP, Yu Q. Designing against size effect on shear strength of reinforced concrete beams without stirrups: I. Formulation. J Struct Engng ASCE 2005;131(12):1877–85.
[31] Hoover CG, Bažant ZP. Comprehensive concrete fracture tests: size effects of types 1 & 2, crack length effect and postpeak. Engng Fract Mech 2013;110:281–9.
[32] ASTM 2010. Standard test method for flexural strength of concrete (using simple beam with center-point loading). C293/C293M 10; 2010.
[33] ACI Committee 209. Guide for modeling and calculating shrinkage and creep in hardened concrete. ACI Report 209.2R-08, Farmington Hills; 2008.
[34] Beygi MHA, Kazemi MT, Nikbin IM, Javad VA. The effect of water to cement ratio on fracture parameters and brittleness of self-compacting concrete. Mat Des 2013;50:267–76.
[35] Hoover CG, Bažant ZP. Comparison of Hu-Duan Boundary Effect Model to Size-Shape Effect Law for Quasibrittle Fracture Based on New Comprehensive Fracture Tests. J Engng Mech, in press.
[36] Bažant ZP, Yu Q. Universal size effect law and effect of crack depth on quasi-brittle structure strength. J Engng Mech 2009;135(2):78–84.
[37] Hoover CG, Bažant ZP. Universal size-shape effect law based on comprehensive concrete fracture tests. J Engng Mech, in press.